



Switchable reinforced streptavidin†

Cite this: DOI: 10.1039/d0nr00265h Leonard C. Schendel, ‡ Steffen M. Sedlak ‡ and Hermann E. Gaub*

The complex of the small molecule biotin and the homotetrameric protein streptavidin is key to a broad range of biotechnological applications. Therefore, the behavior of this extraordinarily high-affinity interaction under mechanical force is intensively studied by single-molecule force spectroscopy. Recently, steered molecular dynamics simulations have identified a low force pathway for the dissociation of biotin from streptavidin, which involves partial unfolding of the N-terminal β -sheet structure of monovalent streptavidin's functional subunit. Based on these results, we now introduced two mutations (T18C,A33C) in the functional subunit of monovalent streptavidin to establish a switchable connection (disulfide bridge) between the first two β -strands to prevent this unfolding. In atomic force microscopy-based single-molecule force spectroscopy experiments, we observed unbinding forces of about 350 pN (at a force-loading rate of 10 nN s⁻¹) for pulling a single biotin out of an N-terminally anchored monovalent streptavidin binding pocket – about 1.5-fold higher compared with what has been reported for N-terminal force loading of native monovalent streptavidin. Upon addition of a reducing agent, the unbinding forces dropped back to 200 pN, as the disulfide bridge was destroyed. Switching from reducing to oxidizing buffer conditions, the inverse effect was observed. Our work illustrates how the mechanics of a receptor–ligand system can be tuned by engineering the receptor protein far off the ligand-binding pocket.

Received 9th January 2020,
Accepted 7th March 2020

DOI: 10.1039/d0nr00265h

rsc.li/nanoscale

Introduction

Many bio- and nanotechnological assays rely on the high-affinity¹ interaction of the small molecule biotin (vitamin H) with the homotetrameric protein streptavidin² (SA). Also, for force spectroscopy, which is an important tool for the emergent research field of mechanobiology,³ the biotin/streptavidin system is abundantly used as a molecular anchor – not only in AFM-based force spectroscopy⁴ but also in acoustic force spectroscopy⁵ as well as magnetic⁶ and optical tweezers⁷ experiments. Therefore, it is important to fundamentally understand the mechanics of the biotin/streptavidin interaction itself.

Using monovalent streptavidin⁸ (mSA), a streptavidin tetramer composed of one functional biotin binding subunit with a unique tethering site and three non-functional subunits, allows for single-molecule force spectroscopy (SMFS) experiments in a well-defined force-loading geometry.⁹ With this approach it has recently been shown that the mechanical stability of the widely used SA/biotin complex differs for N- and C-terminal tethering of the functional subunit of mSA.¹⁰

Compared to N-terminal attachment, the C-terminal one is more than twofold as stable (at force-loading rates of 10 nN s⁻¹). Details of the unbinding process have been investigated using steered molecular dynamics simulations.¹¹ The results suggested that the functional subunit, when SA is pulled by the N-terminus, partially unfolds in the N-terminal region before biotin leaves the binding pocket: The first two N-terminal β -strands β 1 and β 2 are zipped open, destabilizing the binding pocket. This results in lower unbinding forces for biotin compared with C-terminal force loading of mSA. For the significantly different unbinding forces, which have been observed in AFM-based SMFS experiments for N- and C-terminal tethering of mSA, steered molecular dynamics simulations¹⁰ provided an explanation by suggesting the partial unfolding of the N-terminal β -sheet structure. However, this mechanism has not yet been experimentally verified.

An obvious approach to do so is to use protein engineering to introduce a covalent link between β 1 and β 2. Inferring from the steered molecular dynamics simulations, this should block the unbinding pathway that involves partial unfolding of the N-terminal β -sheet structure and thus increase the mechanical stability of the biotin/mSA interaction under mechanical load. Disulfide bridges are a popular choice to establish a covalent link between two β -strands.¹² For human cardiac titin, it was shown that the formation of disulfide bridges between β -strands can modulate the mechanical extensibility of certain domains.^{13,14} Sharma *et al.* successfully used a disulfide

Lehrstuhl für Angewandte Physik and Center for NanoScience, Ludwig-Maximilians-Universität München, Amalienstr. 54, 80799 Munich, Germany.

E-mail: gaub@lmu.de

† Electronic supplementary information (ESI) available. See DOI: 10.1039/d0nr00265h

‡ These authors contributed equally to this work.

bridge to tune the mechanical stability of a *de novo* designed protein.¹⁵ For avidin, which is similar to SA, Nordlund *et al.* succeeded in introducing disulfide bridges between the four subunits to increase the thermal stability of the tetramer.¹⁶ In contrast to previous protein engineering on SA, which mainly focused on the biotin binding pocket^{17–21} or on the assembly of the tetramer,^{8,22–25} the results of the recent steered molecular dynamics simulations inspired us to design a disulfide bridge between the N-terminal β -strands within a single subunit (not in close proximity of the biotin binding pocket) to specifically alter the mechanics of the biotin/mSA interaction. Investigating how a covalent link within the N-terminal β -sheet structure affects the behavior of the biotin/mSA interaction under mechanical force, we provide insights on the interplay of unbinding and unfolding with respect to the dissociation of a ligand from a receptor under mechanical force.

Experimental

Preparation of proteins

Sequences of all protein constructs are provided in the ESI.† Site-directed mutagenesis to obtain the GG-SA(T18C,A33C)-His-construct was performed by three consecutive polymerase chain reactions starting with a Cys-SA-His-construct.¹⁰ Primer sequences and details are provided in the ESI.† To confirm the success of the mutagenesis, all constructs were sent to sequencing (Eurofins Genomics, Ebersberg, Germany). mSA was expressed and purified as described by Sedlak *et al.*¹⁰ In brief, mSA is prepared by mixing two different sorts of subunits that have been expressed separately. The functional subunit SA(T18C,A33C) is equipped with a tag for surface attachment and a tag for purification. The assembly with the non-functional subunits into tetramers is stochastically. During nickel-affinity purification, we select for those that only have one purification-tag (His-Tag) and therefore one functional subunit with one tag for surface attachment.

Sodium dodecyl sulfate-polyacrylamide gel electrophoresis (SDS-PAGE) was employed to confirm mSA's monovalence and purity (*cf.* ESI Fig. S1 and S2†). The presence of the disulfide bridge was probed in a fluorescence anisotropy measurement using a maleimide-dye (ESI Fig. S3†). SdrG was prepared as described by Milles *et al.*²⁶ ddFLN4-constructs were prepared as described by Milles *et al.*²⁷

For biotinylation of the Fg β -ddFLN4-construct, 60 μ M Fg β -ddFLN4-ybbR, 75 μ M Coenzyme A-Biotin, and 5 μ M Sfp phosphopantetheinyl transferase²⁸ were dissolved in Sfp buffer (1 mM MgCl₂, 10 mM Tris, pH 7.5) and incubated at room temperature for 1 h. Subsequently, a buffer exchange to phosphate buffered saline (PBS; Sigma Aldrich, St Louis, USA) was performed using Zeba Spin Desalting Columns (Thermo Fisher Scientific, Waltham, USA) with a 7 kDa molecular weight cut-off according to the manufacturer's instructions.

Isothermal titration calorimetry

Zeba Spin Desalting Columns (Thermo Scientific, Rockford, USA) with a molecular weight cut-off of 40 kDa were employed

to equilibrate reinforced mSA with pure PBS or with PBS containing 1 mM TCEP. For the latter, Bond-Breaker TCEP Solution (Thermo Scientific, Rockford, USA) of neutral pH was added to PBS before the mSA buffer exchange. The final concentration was determined by UV-Vis absorption spectroscopy (NanoDrop 1000, Thermo Scientific, Rockford, USA) using the absorption at 280 nm and a molecular extinction coefficient of 167 760 (without TCEP) or 167 885 (with TCEP) calculated from the amino acid sequence using expASY²⁹ and read 8.34 μ M (without TCEP) and 8.11 μ M (with TCEP), respectively. Biotin was dissolved in PBS (also with and without 1 mM TCEP) to a final concentration of 81.86 μ M. For the ITC measurements with TCEP in the measurement buffer, thus both mSA buffer and biotin buffer contained 1 mM TCEP. ITC measurements were performed at 25 °C on a Malvern MicroCal ITC200 (Malvern Panalytical, Malvern, UK).

Surface and cantilever preparation

Aminosilanized glass slides³⁰ were incubated for 30 min with 25 mM heterobifunctional polyethylene glycol linkers of 5000 Da molecular weight (with an N-hydroxy succinimide group on the one and a maleimide group on the other end; NHS-PEG-MAL) dissolved in 50 mM HEPES buffer at pH 7.5. The glass slides were washed in ultrapure water and then incubated for 1 h with 10 mM Coenzyme A dissolved in coupling buffer (50 mM Na₂HPO₄, 50 mM NaCl, 10 mM EDTA, pH 7.2). The glass slides were again washed in ultrapure water, dried and mounted into the AFM sample holder. The surfaces were then incubated for 1 h with 60 μ M ybbR-ddFLN4-LPETGG and 5 μ M Sfp phosphopantetheinyl transferase²⁸ dissolved in Sfp buffer. The surfaces were washed with PBS and subsequently with Sortase buffer (1 mM MgCl₂, 1 mM CaCl₂, 150 mM NaCl, pH 7.4). Surfaces were incubated for 45 min with 1 μ M GG-mSA(T18C,A33C)-His and 0.2 μ M evolved Sortase A.³¹ Finally, surfaces were washed with coupling buffer and then stored in PBS.

BioLever Mini (Olympus, Tokyo, Japan) were aminosilanized³⁰ and incubated for 30 min with 25 mM NHS-PEG-MAL dissolved in 50 mM HEPES buffer at pH 7.5. Cantilevers were washed in ultrapure water and then incubated for 1 h with 10 mM Coenzyme A dissolved in coupling buffer. Cantilevers were again washed in ultrapure water. Cantilevers were incubated for 1 h with 13 μ M SdrG-ybbR and 5 μ M Sfp phosphopantetheinyl transferase²⁸ dissolved in Sfp buffer. Cantilevers were washed and stored in PBS.

AFM-based SMFS experiments

A custom-built AFM was employed for the AFM-based SMFS experiments. We used a self-written routine programmed in Igor Pro 6 (WaveMetrics, Oregon, USA) to control the MFP-3D controller (Asylum Research, Santa Barbara, USA) operating the AFM. The cantilever tip was shortly indented into the surface (up to 100 pN indentation force) and then retracted 350 nm at constant velocity. Depending on the retraction velocity, tip and surface were in contact for about 0.5 ms to 5 ms. The approach was performed at 3000 nm s⁻¹, the retraction at

200 nm s⁻¹, 800 nm s⁻¹ or 3200 nm s⁻¹. The cantilever deflection was read out at 3000 Hz, 12 000 Hz or 48 000 Hz. To access a fresh surface area, the surface was moved by 100 nm in lateral direction after each approach-retraction cycle. All measurements were performed in PBS, pH 7.4 in ambient conditions. About 1 nM of the Fgβ-ddFLN4-Biotin construct was added to the measurement buffer. After a few thousand approach-retraction cycles, 1 mM Bond-Breaker TCEP Solution (ThermoFisher Scientific, Waltham, USA) was added to the measurement buffer. Independently of the AFM measurement, we ensured that the addition of Bond-Breaker TCEP Solution does not affect the pH of the buffer using indicator paper. For the inverse experiment, *i.e.* starting in reducing conditions and then changing to oxidizing conditions, we first measured in PBS containing TCEP and then exchanged the buffer for PBS without TCEP (instead enriched with oxygen). For calibration of the cantilevers, the thermal noise method as described by te Riet *et al.* was used.³²

AFM-based single-molecule force spectroscopy data analysis

Force–distance traces were obtained by converting z-piezo and deflection voltage using the cantilever spring constant, the optical lever and z-piezo sensitivity. Zero-points are deter-

mined for each force-extension trace and denoising is performed after cantilever bending correction. To detect force peaks, the data are translated into contour length space. Then data are sorted to identify curves that exhibit two distinct two-step unfoldings of the ddFLN4 fingerprint domains. Finally, unfolding and unbinding forces are extracted, plotted as histograms and fitted.

Results and discussion

In this work, we employed protein engineering to establish a covalent link between the two N-terminal β-strands β1 and β2 of mSA's functional subunit. Our intention was to perform AFM-based SMFS experiments, in which we keep the N-terminal β-sheet structure intact while pulling biotin out of mSA's N-terminally tethered functional binding pocket. Based on their position within β1 and β2, their distance and orientation in the crystal structure, we identified threonine 18 and alanine 33 (Fig. 1A) as good candidates for mutations to cysteines. With these two mutations (T18C,A33C), the formation of a disulfide bridge, which connects β1 and β2, thereby preventing the separation of the two, is facilitated.

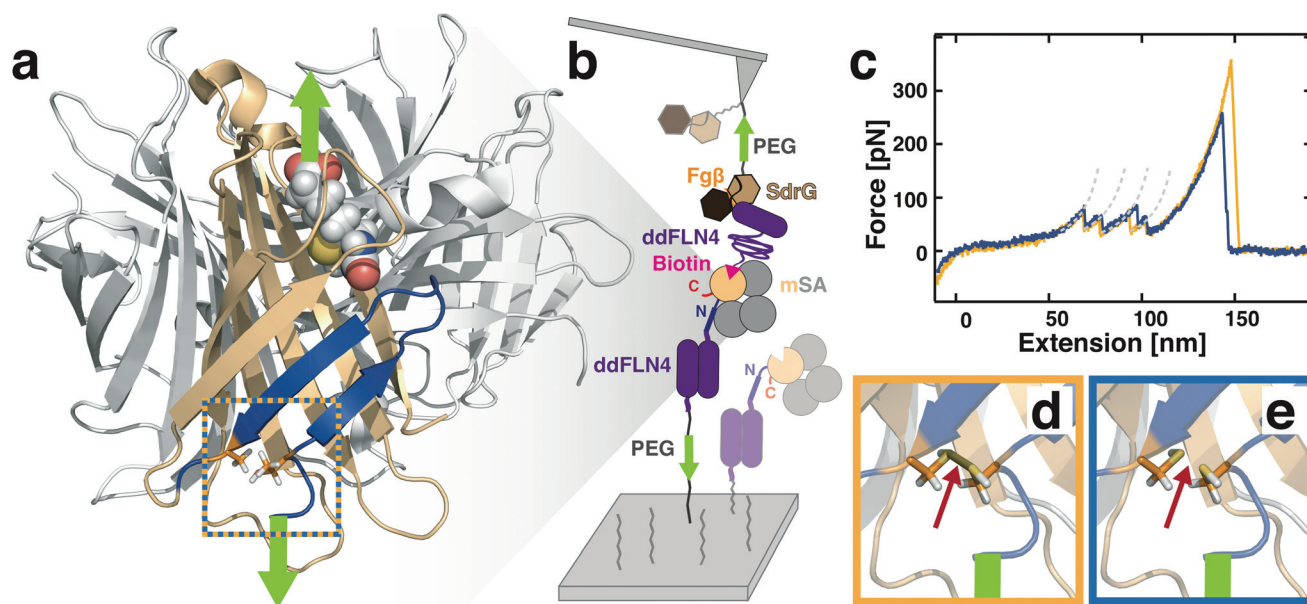


Fig. 1 Protein design and experimental setup. (a) Crystal structure of SA (adapted from PDB:6M9B⁴¹) with biotin (spheres) in one of the binding pockets. Green arrows indicate the attachment points (N-terminus of SA's functional subunit and biotin's carboxyl group), which are pulled apart in the SMFS experiment. The first two N-terminal β-strands, which have been shown to partially unfold prior to the unbinding of biotin are highlighted in blue. Residues T18 and A33, which we mutated to cysteines, are shown in orange stick representation. The colored box encloses the area that is zoomed-in in (d) and (e). (b) Experimental setup. mSA is covalently attached by the N-terminus of the functional subunit to a ddFLN4 fingerprint domain which in turn is tethered by a PEG-linker onto a glass surface. The AFM cantilever tip is functionalized with the SdrG (brown) that binds Fgβ (orange), which is fused to a biotinylated ddFLN4 fingerprint domain bound to the mSA on the surface. Retracting the cantilever from the surface, PEG linkers get stretched until the ddFLN4 fingerprints unfold providing additional contour length. Finally, biotin unbinds from mSA. (c) A typical force extension trace with the two distinct two-step unfolding patterns of ddFLN4 before the biotin/SA unbinding. Grey dashed lines are fits of the worm-like chain model⁴² to the data. Light yellow curve: In the absence of a reducing agent, a disulfide bridge is formed between the mutated residues T18C and A33C (d). Blue curve: In the presence of a reducing agent, the disulfide bridge is destroyed (e), resulting in lower unbinding forces of biotin from mSA. Red arrows in (e) and (d) highlight the position of the intact (d) and destroyed (e) disulfide bridge between the mutated residues T18C and A33C.

We performed isothermal titration calorimetry measurements (*cf.* Fig. 2) to ensure that neither the mutations nor the formation of the disulfide bridge affect biotin binding. For the measurement without TCEP, we observed a binding stoichiometry of $N = (1.19 \pm 0.26)$ and a binding enthalpy of $\Delta H = -(27.2 \pm 3.2)$ kcal mol⁻¹. The measurement with TCEP yielded $N = (1.15 \pm 0.25)$ and $\Delta H = -(26.3 \pm 3.0)$ kcal mol⁻¹. With our instrument a reliable value for the affinity of the binding could not be obtained – only an upper bound of 1 nM can be pro-

vided. Measurement uncertainties were estimated using the min–max method and assuming a 10% uncertainty in the concentrations of both analyte and titrant. Within these uncertainties, the binding enthalpy agrees with literature values for the mSA/biotin interaction.^{9,10,33,34} We conclude that in the absence of mechanical load, the characteristic properties of biotin binding are not altered for our novel mSA mutant. Furthermore, the ITC data also confirms the monovalency of our reinforced mSA.

Previously, an N-terminal cysteine in mSA's functional subunit has always been used for site-specific immobilization on a maleimide-functionalized glass surface.^{9,10,35,36} To prevent any interference with the two newly introduced cysteines, we modified our immobilization chemistry and replaced the N-terminal cysteine by glycine to allow for site-specific surface attachment using a Sortase-mediated linkage.³⁷

For SMFS experiments, we used an elaborate attachment strategy introducing the well-characterized fourth filamin domain of *Dictyostelium discoideum*³⁸ (ddFLN4) as so-called fingerprint domain³⁹ on both sides of the receptor–ligand system (Fig. 1B). Their clear two-step unfolding patterns enable the identification of single-molecule interactions and serve as an internal force reference. The adhesin SD-repeat protein G (SdrG)⁴⁰ is covalently attached to the cantilever tip and binds to a short peptide from human fibrinogen β (Fg β) genetically fused to the biotinylated ddFLN4 that is bound to the mSA on the surface. The use of the SdrG/Fg β system to probe the biotin/mSA interaction has been previously established:¹⁰ the tenfold higher unbinding forces²⁶ of the SdrG/

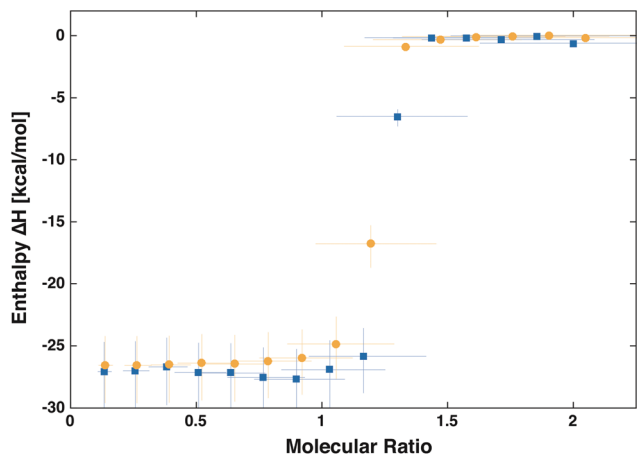


Fig. 2 ITC data for titrating biotin into a solution of the reinforced mSA. Blue squares: without TCEP. Yellow circles: with 1 mM TCEP in both titrant and analyte solution. Error bars are a maximum error estimate assuming a 10% uncertainty in both analyte and titrant concentration.

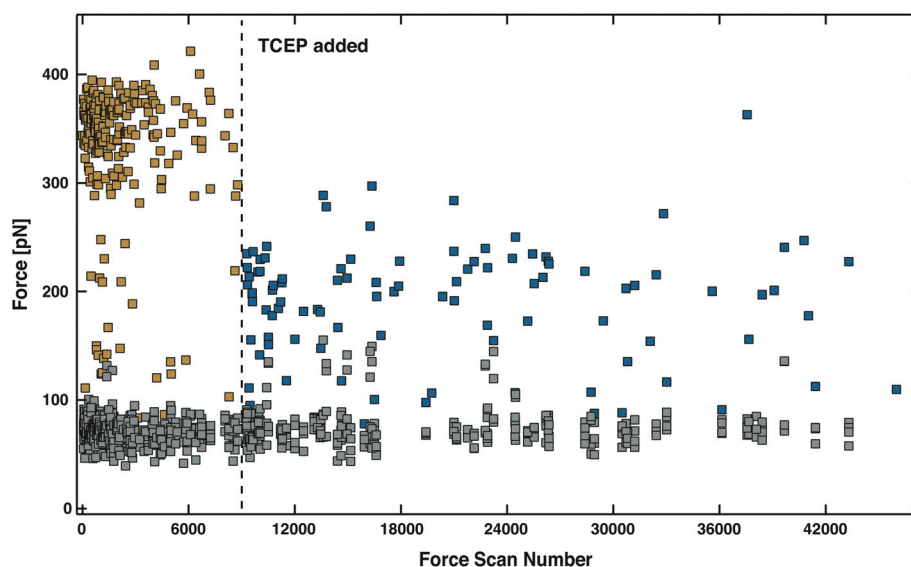


Fig. 3 Course of the AFM-based SMFS measurement. For all force–extension traces recorded at 800 nm s⁻¹ showing two distinct ddFLN4 unfolding pattern before the unbinding of biotin from mSA, the four ddFLN4 unfolding forces (grey) and the final biotin/mSA unbinding force (colored) are plotted over time. After about 9000 approach–retraction cycles, the reducing agent TCEP was added to the measurement buffer (indicated by the dashed line). In the absence of TCEP (yellow), the mSA/biotin unbinding forces are significantly higher than in the presence of TCEP (blue). TCEP does not affect the unfolding forces of ddFLN4. The decrease in interaction frequency over time is independent of TCEP addition and probably due to wear out of the cantilever functionalization.

Fg β system allow to reliably probe the mechanically weaker biotin/mSA interaction, while the lower affinity of SdrG/Fg β system prevents permanent clogging of the cantilever tip.

Retracting the cantilever from the surface, the polyethylene glycol (PEG) linkers, both on the cantilever tip and on the surface, get stretched. At some point, the ddFLN4 fingerprint domains subsequently unfold, adding additional contour length to the stretched polymer chain. Finally, biotin unbinds from mSA. Typical force extension traces are depicted in Fig. 1C.

We probed mSA under two different conditions: without and with a reducing agent in the measurement buffer. In the absence of the reducing agent, we measured about 1.5-fold higher unbinding forces for pulling biotin out of mSA's binding pocket (yellow curve in Fig. 1C) compared with measurements performed in the presence of the reducing agent (blue curve in Fig. 1C).

We attribute this difference in force to two different states of the mSA molecule. With the mutations T18C and A33C, a disulfide bridge connecting β -strands β 1 and β 2 (Fig. 1D) is formed, which is destroyed upon addition of a reducing agent to the measurement buffer. When the reducing agent is added, the covalent linkage between the N-terminal β -strands is lost (Fig. 1E).

In Fig. 3, the temporal course of the SMFS measurement is depicted for the retraction velocity of 800 nm s⁻¹. (Data for other retraction velocities are provided in ESI Fig. S4 and S5.†) Before the addition of TCEP (indicated by the dashed vertical line), unbinding forces are significantly higher. The decrease in interaction frequency over time is probably due to wear out of the cantilever functionalization and independent of the TCEP addition. For the inverse experiment (ESI Fig. S6†), a similar decrease in interaction frequency was observed. Importantly, the unfolding forces of ddFLN4, which serve as an internal force reference, are not affected by the addition of the reducing agent. This confirms that the reducing agent is indeed acting on the mSA/biotin system only.

Rupture force histograms provide yet a better visualization of the data (Fig. 4). In the yellow histograms with peaks at around 350 pN, unbinding forces measured without TCEP in the measurement buffer are plotted. Single events at lower forces, which might be caused by molecules that did not form a disulfide bridge, are also observed. Upon addition of the reducing agent, the forces drop to about 200 pN (blue histograms). This is comparable to what has been measured for N-terminally tethered mSA that does not have the two mutations (T18C,A33C).^{9,10} This finding confirms that with the two mutations (T18C,A33C) a disulfide bridge is formed between β -strands β 1 and β 2 of the functional subunit of mSA. The covalent link prevents the partial unfolding of the N-terminal β -sheet structure under load. Thereby, the unbinding pathway, which involves separation of the N-terminal β -strands, *i.e.* partial unfolding of the functional subunit, is blocked. The disulfide bridge thus helps to preserve the structural integrity of the binding pocket under mechanical load. The mechanical stability of the biotin/mSA

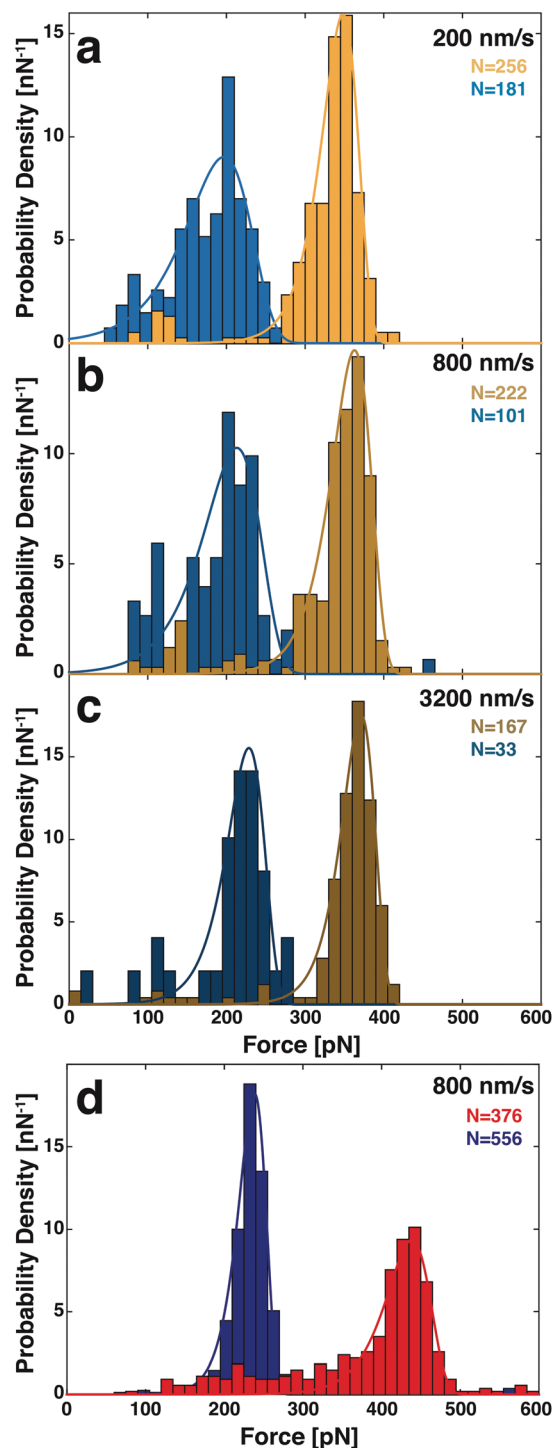


Fig. 4 Force histograms. (a–c) For the same measurement as shown in Fig. 3, histograms of the biotin/mSA unbinding force are plotted for the different cantilever retraction velocities (*i.e.* different force-loading rates). The spring constant of the AFM cantilever read 86 pN nm⁻¹. Unbinding forces measured without the reducing agent TCEP are plotted in yellow, those measured with TCEP in the measurement buffer are plotted in blue. All histograms are fitted with a Bell–Evans distribution. Fit parameters and physical parameters are provided in ESI Tables S1 and S2.† (d) Previously published SMFS data on the mSA/biotin interaction for N- (blue) and C-terminal (red) tethering of mSA without the mutations (T18C,A33C) are shown for comparison. For this measurement, the spring constant of the AFM cantilever was 169 pN nm⁻¹.

interaction is thus increased and higher forces are reached before biotin can overcome the energy barrier and escape from the binding pocket.

For further validation and to illustrate that we can indeed switch between the mechanically weak and the mechanically strong biotin/mSA interaction, we also performed the inverse experiment (ESI Fig. S6†). We first measured the unbinding forces of biotin from the mutated mSA in a reducing environment, *i.e.* with TCEP in the measurement buffer and observed low unbinding forces of about 200 pN. Then, we exchanged the measurement buffer to perform the measurement in an oxidizing environment (using oxygen-enriched PBS). For the vast majority of unbinding events observed under these conditions, we measured forces distributed around 350 pN. Recording this increase in mechanical stability, we deduce that we are indeed monitoring the formation of a disulfide bridge between the mutated amino acids (T18C,A33C).

The forces for unbinding biotin from the N-terminally tethered mSA with the disulfide bridge between the N-terminal β -strands (about 350 pN) are still weaker compared with those that have been reported for SMFS experiments using C-terminal tethering of mSA (about 425 pN).¹⁰ For convenience, we plotted these data in Fig. 4D. (The dynamic force spectra are compared in ESI Fig. S7.†) Compared to the rather broad dispersion of the data recorded for the C-terminally attached mSA, the distributions for the mutated mSA(T18C, A33C) are rather narrow. These variations in force distributions might be due to the difference in tethering geometry and the way biotin and the adjacent linker interact with the L3/4 peptide loop that closes over the binding pocket when the molecular complex is under load, as recently shown by Sedlak *et al.*⁴³ It also illustrates the complexity of unbinding pathways and the strong dependence of mechanical stability on the molecular details. From our SMFS results, it is not possible to exclude that, despite the disulfide bridge, there still is unfolding of the N-terminal β -sheet structure prior to the biotin rupture. The 1.5-fold increase in unbinding force (caused by introduction of the disulfide bridge between the N-terminal β -strands) is yet significant and a convincing argument for the unbinding pathway that involves unfolding prior to unbinding, which has been observed in steered molecular dynamics simulations.¹⁰

Conclusion

In this work, we demonstrate how SMFS stimulated by steered molecular dynamics simulation leads to a deeper understanding of the mechanics of molecular processes and provides guidance for protein engineering with the goal to specifically design the quality of the interaction between biomolecules. With the creation of a disulfide bridge within mSA's N-terminal β -sheet structure, we specifically blocked a certain, comparatively weak, unbinding pathway. Thereby, we significantly increased the mechanical stability of the biotin/mSA interaction. We provided an experimental confirmation for the

molecular pathway previously identified by steered molecular dynamics simulations: under load, N-terminally tethered mSA is partially unfolded before biotin leaves the binding pocket. Thus, we found a prime example for the close interconnection of unfolding and unbinding for receptor–ligand dissociation under mechanical force.

Conflicts of interest

There are no conflicts to declare.

Acknowledgements

This study was inspired by the steered molecular dynamics simulations of R. C. Bernardi and the stimulating discussions with L. F. Milles on the interplay of unfolding and unbinding in protein complexes. The authors thank A. Kardinal and T. Nicolaus for laboratory support and L. F. Milles for providing the SdrG/Fg β -system. The authors acknowledge M. S. Bauer and C. Kluger for helpful discussions. S. M. Sedlak thanks the Nanosystems Initiative Munich for support. This work was funded by the Deutsche Forschungsgemeinschaft (DFG, German Research Foundation) – Project-ID 201269156 – SFB1032.

Notes and references

- 1 N. M. Green, *Methods Enzymol.*, 1990, **184**, 51–67.
- 2 T. Sano, M. W. Pandori, X. Chen, C. L. Smith and C. R. Cantor, *J. Biol. Chem.*, 1995, **270**, 28204–28209.
- 3 M. Krieg, G. Fläschner, D. Alsteens, B. M. Gaub, W. H. Roos, G. J. L. Wuite, H. E. Gaub, C. Gerber, Y. F. Dufrêne and D. J. Müller, *Nat. Rev. Phys.*, 2019, **1**, 41–57.
- 4 G. Sitters, D. Kamsma, G. Thalhammer, M. Ritsch-Marte, E. J. Peterman and G. J. Wuite, *Nat. Methods*, 2015, **12**, 47–50.
- 5 W. Ott, M. A. Jobst, C. Schoeler, H. E. Gaub and M. A. Nash, *J. Struct. Biol.*, 2017, **197**, 3–12.
- 6 A. Lof, P. U. Walker, S. M. Sedlak, S. Gruber, T. Obser, M. A. Brehm, M. Benoit and J. Lipfert, *Proc. Natl. Acad. Sci. U. S. A.*, 2019, **116**, 18798–18807.
- 7 K. M. Tych, M. Jahn, F. Gegenfurtner, V. K. Hechtel, J. Buchner, T. Hugel and M. Rief, *J. Phys. Chem. B*, 2018, **122**, 11373–11380.
- 8 M. Howarth, D. J. Chinnapen, K. Gerrow, P. C. Dorrestein, M. R. Grandy, N. L. Kelleher, A. El-Husseini and A. Y. Ting, *Nat. Methods*, 2006, **3**, 267–273.
- 9 S. M. Sedlak, M. S. Bauer, C. Kluger, L. C. Schendel, L. F. Milles, D. A. Pippig and H. E. Gaub, *PLoS One*, 2017, **12**, e0188722.
- 10 S. M. Sedlak, L. C. Schendel, M. C. R. Melo, D. A. Pippig, Z. Luthey-Schulten, H. E. Gaub and R. C. Bernardi, *Nano Lett.*, 2019, **19**, 3415–3421.

- 11 W. Humphrey, A. Dalke and K. Schulten, *J. Mol. Graphics*, 1996, **14**, 33–38, 27–38.
- 12 A. A. Dombkowski, K. Z. Sultana and D. B. Craig, *FEBS Lett.*, 2014, **588**, 206–212.
- 13 H. Li and J. M. Fernandez, *J. Mol. Biol.*, 2003, **334**, 75–86.
- 14 A. Grutzner, S. Garcia-Manyes, S. Kotter, C. L. Badilla, J. M. Fernandez and W. A. Linke, *Biophys. J.*, 2009, **97**, 825–834.
- 15 D. Sharma, O. Perisic, Q. Peng, Y. Cao, C. Lam, H. Lu and H. Li, *Proc. Natl. Acad. Sci. U. S. A.*, 2007, **104**, 9278–9283.
- 16 H. R. Nordlund, O. H. Laitinen, S. T. Uotila, T. Nyholm, V. P. Hytonen, J. P. Slotte and M. S. Kulomaa, *J. Biol. Chem.*, 2003, **278**, 2479–2483.
- 17 A. Chilkoti, T. Boland, B. D. Ratner and P. S. Stayton, *Biophys. J.*, 1995, **69**, 2125–2130.
- 18 S. Voss and A. Skerra, *Protein Eng., Des. Sel.*, 1997, **10**, 975–982.
- 19 G. O. Reznik, S. Vajda, T. Sano and C. R. Cantor, *Proc. Natl. Acad. Sci. U. S. A.*, 1998, **95**, 13525–13530.
- 20 I. P. Korndorfer and A. Skerra, *Protein Sci.*, 2002, **11**, 883–893.
- 21 C. E. Chivers, E. Crozat, C. Chu, V. T. Moy, D. J. Sherratt and M. Howarth, *Nat. Methods*, 2010, **7**, 391–393.
- 22 K. H. Lim, H. Huang, A. Pralle and S. Park, *Biotechnol. Bioeng.*, 2013, **110**, 57–67.
- 23 D. DeMonte, E. J. Drake, K. H. Lim, A. M. Gulick and S. Park, *Proteins: Struct., Funct., Bioinf.*, 2013, **81**, 1621–1633.
- 24 D. Demonte, C. M. Dundas and S. Park, *Appl. Microbiol. Biotechnol.*, 2014, **98**, 6285–6295.
- 25 M. Fairhead, D. Krndija, E. D. Lowe and M. Howarth, *J. Mol. Biol.*, 2014, **426**, 199–214.
- 26 L. F. Milles, K. Schulten, H. E. Gaub and R. C. Bernardi, *Science*, 2018, **359**, 1527–1533.
- 27 L. F. Milles, E. A. Bayer, M. A. Nash and H. E. Gaub, *J. Phys. Chem. B*, 2017, **121**, 3620–3625.
- 28 J. Yin, P. D. Straight, S. M. McLoughlin, Z. Zhou, A. J. Lin, D. E. Golan, N. L. Kelleher, R. Kolter and C. T. Walsh, *Proc. Natl. Acad. Sci. U. S. A.*, 2005, **102**, 15815–15820.
- 29 P. Artimo, M. Jonnalagedda, K. Arnold, D. Baratin, G. Csardi, E. de Castro, S. Duvaud, V. Flegel, A. Fortier, E. Gasteiger, A. Grosdidier, C. Hernandez, V. Ioannidis, D. Kuznetsov, R. Liechti, S. Moretti, K. Mostaguir, N. Redaschi, G. Rossier, I. Xenarios and H. Stockinger, *Nucleic Acids Res.*, 2012, **40**, W597–W603.
- 30 J. L. Zimmermann, T. Nicolaus, G. Neuert and K. Blank, *Nat. Protoc.*, 2010, **5**, 975–985.
- 31 I. Chen, B. M. Dorr and D. R. Liu, *Proc. Natl. Acad. Sci. U. S. A.*, 2011, **108**, 11399–11404.
- 32 J. te Riet, A. J. Katan, C. Rankl, S. W. Stahl, A. M. van Buul, I. Y. Phang, A. Gomez-Casado, P. Schon, J. W. Gerritsen, A. Cambi, A. E. Rowan, G. J. Vancso, P. Jonkheijm, J. Huskens, T. H. Oosterkamp, H. Gaub, P. Hinterdorfer, C. G. Figdor and S. Speller, *Ultramicroscopy*, 2011, **111**, 1659–1669.
- 33 A. Chilkoti and P. S. Stayton, *J. Am. Chem. Soc.*, 1995, **117**, 10622–10628.
- 34 M. Sarter, D. Niether, B. W. Koenig, W. Lohstroh, M. Zamponi, N. H. Jalarvo, S. Wiegand, J. Fitter and A. M. Stadler, *J. Phys. Chem. B*, 2020, **124**, 324–335.
- 35 F. Baumann, M. S. Bauer, L. F. Milles, A. Alexandrovich, H. E. Gaub and D. A. Pippig, *Nat. Nanotechnol.*, 2016, **11**, 89–94.
- 36 K. R. Erlich, S. M. Sedlak, M. A. Jobst, L. F. Milles and H. E. Gaub, *Nanoscale*, 2019, **11**, 407–411.
- 37 E. Durner, W. Ott, M. A. Nash and H. E. Gaub, *ACS Omega*, 2017, **2**, 3064–3069.
- 38 I. Schwaiger, A. Kardinal, M. Schleicher, A. A. Noegel and M. Rief, *Nat. Struct. Mol. Biol.*, 2004, **11**, 81–85.
- 39 M. S. Bauer, L. F. Milles, S. M. Sedlak and H. E. Gaub, *bioRxiv*, 2018.
- 40 P. Herman, S. El-Kirat-Chatel, A. Beaussart, J. A. Geoghegan, T. J. Foster and Y. F. Dufrene, *Mol. Microbiol.*, 2014, **93**, 356–368.
- 41 S. Basu, A. Finke, L. Vera, M. Wang and V. Olieric, *Acta Crystallogr., Sect. D: Struct. Biol.*, 2019, **75**, 262–271.
- 42 C. Bustamante, J. F. Marko, E. D. Siggia and S. Smith, *Science*, 1994, **265**, 1599.
- 43 S. M. Sedlak, L. C. Schendel, H. E. Gaub and R. C. Bernardi, *Sci. Adv.*, 2020, **6**, eaay5999.